Title
Proteasome regulation by reversible tyrosine phosphorylation at the membrane

Journal
Oncogene, 40(11)

ISSN
0950-9232

Authors
Chen, Lu
Zhang, Yanan
Shu, Xin
et al.

Publication Date
2021-03-18

DOI
10.1038/s41388-021-01674-z

Peer reviewed

HHS Public Access

Author manuscript

Oncogene. Author manuscript; available in PMC 2021 March 24.

Published in final edited form as:

Oncogene. 2021 March ; 40(11): 1942–1956. doi:10.1038/s41388-021-01674-z.

Proteasome Regulation by Reversible Tyrosine Phosphorylation at the Membrane

Lu Chen[1,#], **Yanan Zhang**[1,#], **Xin Shu**[1], **Qiong Chen**[1], **Tiantian Wei**[2], **Heman Wang**[1], **Xiaorong Wang**[3], **Qirou Wu**[1], **Xiaomei Zhang**[1], **Xiaoyan Liu**[1], **Suya Zheng**[1], **Lan Huang**[3], **Junyu Xiao**[2], **Chao Jiang**[1], **Bing Yang**[1], **Zhiping Wang**[4,5], **Xing Guo**[1,5]

[1]Zhejiang Provincial Key Laboratory for Cancer Molecular Cell Biology, Life Sciences Institute, Zhejiang University, Hangzhou, China 310058

[2]Academy for Advanced Interdisciplinary Studies, Peking-Tsinghua Center for Life Sciences, Peking University, Beijing, China 100871

[3]Departments of Physiology and Biophysics and of Developmental and Cell Biology, University of California, Irvine, CA, USA 92697

[4]Center for Neuroscience and Department of Neurology of Second Affiliated Hospital, NHC and CAMS Key Laboratory of Medical Neurobiology, Zhejiang University School of Medicine, Hangzhou, China 310058

Abstract

Reversible phosphorylation has emerged as an important mechanism for regulating 26S proteasome function in health and disease. Over 100 phospho-tyrosine (pTyr) sites of the human proteasome have been detected, and yet their function and regulation remain poorly understood. Here we show that the 19S subunit Rpt2 is phosphorylated at Tyr439, a strictly conserved residue within the C-terminal HbYX motif of Rpt2 that is essential for 26S proteasome assembly. Unexpectedly, we found that Y439 phosphorylation depends on Rpt2 membrane localization mediated by its N-myristoylation. Multiple receptor tyrosine kinases (RTKs) can trigger Rpt2-Y439 phosphorylation by activating Src, a N-myristoylated tyrosine kinase. Src directly phosphorylates Rpt2-Y439 *in vitro* and negatively regulates 26S proteasome activity at cellular membranes, which can be reversed by the membrane-associated isoform of protein tyrosine phosphatase non-receptor type 2 (PTPN2). In H1975 lung cancer cells with activated Src, blocking Rpt2-Y439 phosphorylation by the Y439F mutation conferred partial resistance to the Src inhibitor saracatinib both *in vitro* and in a mouse xenograft tumor model, and caused significant changes of cellular responses to saracatinib at the proteome level. Our study has defined a novel mechanism involved in the spatial regulation of proteasome function and provided new insights into tyrosine kinase inhibitor-based anti-cancer therapies.

[5]Corresponding authors. X. G. (xguo@zju.edu.cn), Z. W. (z4wang@zju.edu.cn).
[#]These authors contributed equally to this work.

Declaration of competing interest

The authors declare that they have no competing interests.

Keywords

proteasome; Rpt2/PSMC1; tyrosine phosphorylation; Src; PTPN2

Introduction

The 26S proteasome plays a central role in selective protein degradation in eukaryotic cells and its function is intricately regulated in health and disease [1–3]. Consisting of at least 33 unique subunits, the 26S proteasome can be divided into two large subcomplexes, the 19S regulatory particle (RP) and the 20S core particle (CP). The 20S CP is formed by the stacking of four ring-shaped structures, each comprising seven α subunits (α1–7) or seven β subunits (β1–7), in an α-β-β-α order. N-terminal sequences of the α subunits form a gate at the center of the α ring, restricting substrate access to the catalytic core embedded inside the CP chamber. Gate-opening is achieved by binding of the 19S RP or other proteasome activators to the CP [4, 5].

The 19S RP contains six AAA^+-type ATPase subunits (Rpt1–6) and thirteen non-ATPase subunits (Rpn1–3, 5–13 and 15). They are crucial for substrate engagement, processing and translocation [6, 7]. Rpt1–6 are assembled into a heterohexameric ring that directly docks on the α ring of CP. The C-terminal tails of Rpt1–6, which are highly conserved through evolution, can insert into cognate pockets formed by adjacent α subunits along the α ring. In particular, Rpt2, 3 and 5 have a signature HbYX motif (hydrophobic residue-tyrosine-any amino acid) at their very C-termini, featuring an invariant tyrosine residue at the penultimate position. Numerous genetic, biochemical and structural studies have demonstrated the critical importance of the Rpt tails for proteasome assembly, activity and cell viability [8–12].

Reversible phosphorylation has emerged as an important mechanism for fine-tuning proteasome assembly, activity and subcellular localization [13, 14]. Hundreds of phosphorylation sites have been found on the human 26S proteasome by mass spectrometry, nearly a third of which (143/453) are phospho-tyrosine (pTyr) sites [13]. However, studies on proteasome tyrosine phosphorylation have been extremely limited [15, 16]. A common theme from most phospho-proteomic investigations is that tyrosine phosphorylation of the proteasome mostly occurs in cancer cells with aberrant tyrosine kinase (TK) signaling [13].

Hyperactivated phosphotyrosine signaling can lead to tumorigenesis [17, 18]. Inhibitors against receptor tyrosine kinases (RTKs, e.g. EGFR) and non-receptor tyrosine kinases downstream of the RTKs (such as Src and Abl) have been important components of targeted therapies against cancer [19, 20]. However, even in the presence of activated TKs, phospho-tyrosine levels are usually kept low [21] by protein tyrosine phosphatases (PTPs, [22, 23]). PTPs have also been implicated in oncogenesis and can now be pharmacologically targeted, representing a new approach for anti-cancer treatment [24–26]

In this study, we focused on Src- and PTPN2-regulated phosphorylation of the 19S subunit Rpt2. A shared feature between Src and Rpt2 is that they are both co-translationally modified by N-myristoylation, which usually occurs on N-terminal glycine and targets

proteins to the membrane [27]. PTPN2, also known as T cell PTP (TC-PTP), has multiple splicing isoforms. The longest isoform (called TC48) contains a membrane-targeting region that is absent in the other isoforms [28]. We found that Src and PTPN2 (TC48) control the phosphorylation of membrane-tethered Rpt2 at Tyr439, which is the very tyrosine residue within the HbYX motif critical for 20S association. Src downregulates 26S proteasome activity at the membrane, while lung cancer cells expressing the non-phosphorylatable Rpt2-Y439F mutant are more resistant to Src inhibition *in vitro and in vivo*. These findings have revealed a new mechanism of spatial regulation of the proteasome, and suggest a considerable role of proteasome phosphorylation in determining the clinical outcome of tyrosine kinase inhibitors (TKIs).

Results

Rpt2-Y439 phosphorylation impairs 26S proteasome activity.

According to the PhosphoSitePlus database (www.phosphosite.org), Rpt2-Y439 is the most frequently detected pTyr site of all 19S subunits. Y439 is the exact tyrosine residue of the C-terminal HbYX motif of Rpt2 ($L^{438}\underline{Y}^{439}L^{440}$), which is strictly conserved among species (Fig. 1A). Consistent with the proteomic results, the Y439F mutation largely diminished total pTyr signal of Rpt2 (Supplementary Fig. S1A). To confirm the occurrence of Rpt2-Y439 phosphorylation, we generated a phospho-specific antibody against this site. Ectopically expressed wild-type Rpt2 with an internal Flag tag ("IF", see below), but not the Rpt2-IF-Y439F mutant, was found to be Y439-phosphorylated following anti-Flag immunoprecipitation (Fig. 1B). In 293T cells and H1975 (human lung cancer) cells, endogenous Rpt2-Y439 phosphorylation could be detected following treatment of pervanadate, a potent generic inhibitor of PTPs (Supplementary Fig. S1B, C). Y439-phosphorylated endogenous Rpt2 could also be co-purified with TBHA-tagged Rpn1 subunit [29, 30] of the 19S RP (Fig. 1C). Moreover, Y439 phosphorylation was evident on endogenous Rpt2 from rat embryonic forebrain tissues, while it was barely detectable in the midbrain from the same embryos (Fig. 1D). These initial characterizations indicate that Rpt2-Y439 phosphorylation does occur in cultured cells and *in vivo*, while its level may be dynamically regulated in different cell types or under different conditions.

From all previous studies and our structural modeling (Fig. 1E), it is immediately conceivable that Y439 phosphorylation should be incompatible with Rpt2-CP association due to a steric clash between the Rpt2 tail and the cognate pocket formed by α3 and α4. To examine the consequence of Rpt2-Y439 phosphorylation, we engineered stable cell lines in which endogenous Rpt2 was knocked down by shRNA and simultaneously replaced with WT or mutant Rpt2-IF, with all Rpt2 variants equally expressed at near-physiological levels (Fig. 1F–H). In proteasome pulldown assays with α3-TBHA, the phosphomimetic mutant Rpt2-Y439E showed poor interaction with α3/20S, while the phospho-deficient Rpt2-Y439F remained capable of binding the CP (Fig. 1I). Conversely, in Rpn11-TBHA pulldown assays, WT Rpt2 and both of the Y439 mutants appeared to be well incorporated into the 19S RP, but the amount of associated 20S was largely reduced in Rpt2-Y439E cells (Supplementary Fig. S1D). Consistent with its defect in mediating RP-CP interaction, the Rpt2-Y439E mutant caused a significant inhibition of proteasome activity as compared to

Rpt2-WT or Y439F (Fig. 1J). These results support the notion that Rpt2-Y439 phosphorylation may block RP-CP association and attenuate proteasome activity.

Rpt2-Y439 phosphorylation occurs at the membrane

We then investigated how Rpt2-Y439 phosphorylation is regulated in cells and made a surprising discovery that Rpt2 tyrosine phosphorylation depends on its membrane localization. In our parallel study focusing on Rpt2 N-myristoylation, we engineered the expression construct of Rpt2-IF mentioned above, where aa. 85–91 of WT Rpt2 (MKPLEEK, an unstructured region, [31]) was replaced by the Flag tag sequence, DYKDDDDK (Fig. 2A). This preserves Rpt2 N-myristoylation, an absolutely conserved co-translational modification ([27, 32–38], Supplementary Fig. S2A) that is occluded in the commonly used N-terminally tagged Flag-Rpt2. Rpt2-IF could be similarly incorporated into the 26S proteasome as endogenous Rpt2 and fully support proteasome functions, and was indistinguishable from Flag-Rpt2 in protein expression (Supplementary Fig. S2B–F). Strikingly, however, Rpt2-IF showed much stronger overall tyrosine phosphorylation and Y439 phosphorylation than Flag-Rpt2 (Fig. 2B). For this reason, Rpt2-IF was used throughout this study.

Proteasomes are known to associate with different membranes of the cell [39–41]. Both CP and RP subunits were detected in the membrane fraction by western blot (Fig. 2C). Wild-type Rpt2-IF extensively co-localized with the membrane marker PH-GFP (green fluorescent protein fused to the pleckstrin homology domain), as did the Y439F and Y439E mutants (Supplementary Fig. S2G). By contrast, myristoylation-deficient Rpt2-IF mutants (ΔG and G2A, [34]) completely lost their membrane localization, and their tyrosine phosphorylation (including pY439) was concurrently abrogated (Fig. 2C–E). The same was true for a putative splicing variant of Rpt2 (NP_001317141) missing the N-terminal 73 amino acids of the full-length protein (Fig. 2F). On the contrary, tyrosine phosphorylation of Rpt2-IF-ΔG was fully restored by fusing the myristoylation sequence of Src [42] to its N-terminus (Fig. 2F). Furthermore, endogenous Rpt2-pY439 signal was predominantly found in the membrane fraction (Fig. 2G). These results demonstrate that Rpt2-Y439 phosphorylation depends on its N-terminal myristoylation and occurs primarily at membrane structures of the cell (Fig. 2H).

Src phosphorylates Rpt2-Y439

Next, we set out to search for the Rpt2-Y439 kinase(s), presumably a membrane-localized protein. As an important hint, the EGFR inhibitor gefitinib (Iressa®) completely suppressed Rpt2-Y439 phosphorylation in H3255 non-small cell lung cancer (NSCLC) cells without affecting other phospho-tyrosine sites of the proteasome [43]. We confirmed this phenomenon by western blot (Supplementary Fig. S3A) and observed a similar effect with the third-generation EGFR inhibitor, osimertinib (AZD9291, Tagrisso®), in the aforementioned H1975 NSCLC cells that bear the EGFR-L858R/T790M mutations ([44], Supplementary Fig. S3B). Y439 phosphorylation of endogenous Rpt2 could be enhanced by EGF in both 293T and H1975 cells (Supplementary Fig. S3C), with the latter showing a higher basal level of pY439 likely due to EGFR hyperactivation. Overexpression of several other RTKs such as PDGFRβ, FGFR1, FGFR3, RET and NTRK1 also markedly enhanced

Rpt2-Y439 phosphorylation (Fig. 3A). Therefore, induction of pY439 is not unique to EGFR but seems to be mediated by a common effector downstream various RTKs. Interestingly, RTK-stimulated Y439 phosphorylation was completely blocked by Src inhibitors such as saracatinib/AZD0530 or PP1 (Fig. 3A). Pervanadate-induced pY439 was also fully suppressed by Src inhibitors saracatinib, PP1 or dasatinib (Sprycel®), but not the Abl kinase inhibitor imatinib (Gleevec®) (Fig. 3B). This suggests that Src and/or Src family kinases (SFKs) are responsible for Rpt2-Y439 phosphorylation.

We focused on Src, the primary target of saracatinib [45]. Indeed, ectopic expression of wild-type Src and its constitutively active form Src-Y530F in 293T cells greatly increased Rpt2-Y439 phosphorylation, while the kinase-deficient mutant Src-K298M failed to do so (Fig. 3C). Src co-precipitated with the proteasome from cells (Supplementary Fig. S3D) and directly phosphorylated recombinant Rpt2 at Y439 *in vitro* (Fig. 3D and Supplementary Fig. S3E). Notably, Src itself is also membrane-anchored via N-myristoylation [46] and colocalizes with Rpt2-WT but not Rpt2-G2A at membranes (Fig. 3E). As expected, a Src mutant lacking its N-terminal myristoylation sequence ($Src^{\Delta Myr}$) was much less active toward Rpt2-Y439 than the wild-type kinase (Fig. 3C). These results provided an explanation for the dependence of Y439 phosphorylation on Rpt2 membrane localization. To further assess the activity of membrane-associated proteasomes, we generated a membrane-targeted version of the commonly used proteasome activity reporter GFPodc [47]. This new reporter, designated Myr^{Rpt2}-GFPodc, contains the N-terminal myristoylation sequence of Rpt2 (aa. 1–24) and could be successfully targeted to the membrane and degraded by the proteasome (Supplementary Fig. S3F, G). Src inhibition by saracatinib not only reduced the steady-state level of Myr^{Rpt2}-GFPodc but also greatly accelerated its protein degradation (Fig. 3F and Supplementary Fig. S3H). On the contrary, overexpression of activated Src essentially blocked Myr^{Rpt2}-GFPodc degradation (Fig. 3G and Supplementary Fig. S3H). These data have identified Src as a novel proteasome kinase that phosphorylates Rpt2-Y439 and regulates proteasome activity at the membrane.

PTPN2 dephosphorylates Rpt2-pY439

Previously we identified PTPN2/TC-PTP as a proteasome-interacting protein using Rpn11-HTBH pulldown followed by mass spectrometry, and the result was confirmed by western blot (Supplementary Fig. S4A). Three other proteomic studies also documented such interaction using PTPN2 as bait ([48–50], Supplementary Fig. S4B). Endogenous proteasome subunits preferentially interacted with the membrane-associated isoform of PTPN2 (TC48) but exhibited little binding with the nuclear form, TC45 (Fig. 4A and Supplementary Fig. S4C). Fluorescence microscopy studies also confirmed partial co-localization between GFP-TC48 and Rpt2-WT (but not Rpt2-G2A) in cells (Supplementary Fig. S4D). These results prompted us to test whether PTPN2 regulates Rpt2 phosphorylation.

CRISPR/Cas9-mediated PTPN2 knockout led to an elevation of Rpt2-pY439 in cells (Fig. 4B). Since PTPN2 dephosphorylates and inactivates Src [51], the increase of pY439 might have resulted from reduced dephosphorylation or elevated Src activity or both. To further dissect the role of PTPN2 in Rpt2 regulation, we co-expressed Rpt2 with activated Src to

achieve a high starting level of pY439, then inhibited Src activity by saracatinib and monitored the rate of pY439 disappearance afterwards. In PTPN2-null cells, Src induced strong Rpt2-Y439 phosphorylation that gradually decreased with the addition of saracatinib, while re-expression of TC48 markedly accelerated the decline of pY439 (Fig. 4C). This result supports a direct role of PTPN2/TC48 in controlling Rpt2-pY439 in cells. *In vitro* phosphatase assays further demonstrated that Rpt2 is a direct substrate of PTPN2 (Fig. 4D and Supplementary Fig. S4E). Consistently, TC48 knockdown decreased proteasome peptidase activity in cells, while depletion of TC45 had little affect (Fig. 4E). Furthermore, inhibiting PTPN2 with Compound 8 [52] impeded Myr^{Rpt2}-GFPodc clearance in Rpt2-WT cells, while such effect was lost in the Rpt2-Y439F cells (Fig. 4F). Therefore, Rpt2-pY439 appears to be a major target through which PTPN2 positively regulates proteasome activity.

Rpt2-Y439F mutation lowers cell sensitivity to saracatinib

To further explore the functional importance of Y439 phosphorylation, we turned to the H1975 cells, in which Src is activated by mutated EGFR and Rpt2-Y439 phosphorylation was effectively inhibited by saracatinib (Supplementary Fig. S5A). Rpt2-IF-WT or Y439F were stably introduced using the same knockdown-addback approach and were expressed at similar levels comparable to that of endogenous Rpt2 in H1975 parental cells (Fig. 1F–H). Saracatinib treatment clearly suppressed the viability of H1975-WT cells in colony formation assays in a dose-dependent manner (Fig. 5A). However, although H1975-YF cells were also growth-inhibited, they were apparently less sensitive to saracatinib (Fig. 5A). We surveyed several survival/proliferation-related proteins. p53 was induced by saracatinib in both cell lines, whereas the level of cleaved PARP1 was higher in H1975-WT cells, indicating increased apoptosis (Fig. 5B). On the other hand, CDK4/cyclin D1 were maintained at higher levels in H1975-YF cells after saracatinib treatment, and CDK2 activation was also more evident in the YF cells probably due to elevated expression of cyclin H (Fig. 5B). These differences are consistent with the reduced sensitivity of H1975-YF cells to saracatinib, although they are probably indirect results of saracatinib-mediated proteasome activation at the membrane.

To gain further insight into the role of Rpt2-Y439 phosphorylation in mediating cellular responses to saracatinib, we compared saracatinib-induced whole proteome changes between H1975-WT and YF cells using label-free mass spectrometry (Fig. 5C). From three biological repeats we identified 3036 overlapping proteins (Table S1). In every repeat, saracatinib caused upregulation of 200~300 proteins in each cell line (> 2-fold change in intensity), and a similar number of proteins were downregulated (< 0.5-fold). We assigned a D-score of +1, 0 or −1 to each upregulated, unchanged or downregulated protein, respectively, in every experiment. By summing the D-scores (D_{sum}) from three repeats, we found 280 proteins that were upregulated or downregulated by saracatinib in at least two of the three runs (Table S2). Among them, 69 proteins consistently decreased in WT cells in response to saracatinib, the majority of which (41/69, 60%) are annotated as membrane-localized (www.uniprot.org). However, most of these proteins (64/69) were not downregulated in the YF cells, and *vice versa* (Fig. 5C and Table S3). Saracatinib-upregulated proteins also minimally overlapped between WT and YF cells (Fig. 5C and

Table S4). These findings demonstrate that the Y439F mutation had a profound impact on proteomic changes induced by saracatinib in H1975 cells.

Supporting this notion, western blot analysis of RRas, PAK1, Legumain and Na^+/K^+-ATPase confirmed their downregulation in saracatinib-treated H1975-WT cells but not in H1975-YF cells (Fig. 5D). These proteins have been regarded as pro-tumorigenic and/or anti-cancer drug targets [53–56], and they are among 191 proteins that showed different responses to saracatinib between the two cell lines (defined as $|D_{sum\ (WT)} - D_{sum\ (YF)}| \geq 2$, Fig. 5E and Table S5). Gene Ontology (GO) analysis of these proteins again showed that they are enriched in membrane structures of the cell (Fig. 5F) and involved in various biological processes (Supplementary Fig. S5B, C). These 191 proteins could be assigned to 4 groups (I – IV) based on their expression patterns following saracatinib treatment (Fig. 5E). Of particular interest were proteins that were selectively downregulated (Group I) or less upregulated in WT cells (Group II), which could be substrates of membrane proteasomes (Supplementary Fig. S5D) and were more efficiently degraded in H1975-WT cells following saracatinib treatment. Importantly, our literature search showed that the majority of these Group I/II proteins are considered pro-survival and/or oncogenic. Their downregulation in WT cells is in agreement with the cytotoxic activity of saracatinib, whereas the weakened or opposite changes of these proteins in the YF cells may underlie the elevated resistance to saracatinib as seen above.

H1975-YF tumors gain partial resistance to saracatinib

Saracatinib is currently in Phase 2/3 clinical trials against several types of solid tumors. In a mouse xenograft study with the above H1975 cells (Fig. 6A, [57]), orally administered saracatinib inhibited Src activation in tumor tissues (Fig. 6B) and reduced tumor growth in nude mice (Fig. 6C, D). However, the tumorigenic growth of H1975-YF cells was less suppressed by saracatinib than that of the H1975-WT cells (Fig. 6C, D), echoing results from the colony formation assays (Fig. 5A). Western blot analysis of tumor homogenates again revealed different ramifications of drug treatment in WT and YF tumors. Saracatinib caused a decrease of CDK4, RRas, Legumain and the cell surface molecule CD46/MCP in WT tumors but not in the YF tumors (Fig. 6E), consistent with the mass spectrometry study using cultured cells. Pro-tumorigenic kinases CDK2, Erk1/2 and PAK1 were also more active or present at higher amounts in YF tumors than in WT tumors after saracatinib treatment (Fig. 6E). These differences might at least in part account for the dampened effect of saracatinib on the growth of YF tumors. Taken together, these *in vivo* data further underscore the importance of Rpt2-Y439 phosphorylation in determining cellular sensitivity and responses to saracatinib (Fig. 6F). This form of proteasome regulation may thus be a clinically relevant mechanism that can be tapped to improve the outcome of TKI-based anti-cancer therapies.

Discussion

Proteasome tyrosine phosphorylation has been known for a long time [58] and constitutes a surprisingly high proportion of the proteasome phosphoproteome [13]. However, its functional importance has been unclear largely due to the difficulty of detection by

immunoblotting in unstimulated cells [15, 16, 59, 60]. This is not unexpected because pTyr level in the cell is under tight spatiotemporal control by TKs and PTPs [17, 61]. Here we have identified the kinase, phosphatase and location that together regulate Rpt2-Y439 phosphorylation. Although Rpt2-Y439 is conserved through evolution, its phosphorylation was presumably introduced in metazoans given the apparent lack of canonical tyrosine kinases in yeast [62]. Different from HbYX deletions used in previous studies [11, 63], Y439 phosphorylation of wild-type Rpt2 introduces considerable changes to the tyrosine side chain that is bound to interfere with RP-CP association. The occurrence of Y439 phosphorylation indicates the existence of a pool of endogenous Rpt2 outside the fully assembled 26S proteasomes (e.g. in free 19S RP or subcomplexes), whose Y439 is accessible to kinases such as Src. This may be particularly true for cancer cells like H1975 and H3255 used in this study, both of which contain an extra copy of the *PSMC1* gene (encoding Rpt2, from the Cancer Cell Line Encyclopedia database). As proteasome composition dynamically changes in cells [4, 5, 64–68], Rpt2-Y439 phosphorylation may serve as an assembly checkpoint or prevent re-association of Rpt2/RP with CP after they dissociate.

The dependence of Rpt2-Y439 phosphorylation on Rpt2 membrane localization was unexpected and also intriguing. N-myristoylation of Rpt2 is conserved from yeast to human, and Rpt2 is the only proteasome subunit that begins with Met-Gly, hence the only subunit that can undergo such modification. As found in many myristoylated proteins, a stretch of conserved basic residues is also present near the Rpt2 N-terminus, which may be necessary for securing the membrane association (Supplementary Fig. S2A). In yeast, Rpt2 N-myristoylation has been reported to localize proteasomes to the nuclear envelope [34, 35]. In human cells, Rpt2 is one of the most myristoylated proteins [27], representing an ideal and perhaps prevalent mechanism for targeting proteasomes to the membrane. At the membrane, Rpt2-Y439 can gain access to the nearby TKs such as Src, and extracellular signals can then impinge upon membrane-associated proteasomes, causing changes of the local proteome (Fig. 6F). In addition to its role in tumorigenesis, Rpt2-Y439 phosphorylation in the developing brain (Fig. 1D) may also regulate membrane protein turnover during neuronal cell migration and synapse formation. To our knowledge, Rpt2-Y439 phosphorylation is the first evidence of phosphoregulation of membrane-associated proteasomes, providing important support to the concept of compartmentalized proteasomal degradation.

Membrane localization of Rpt2 is necessary but not sufficient for Y439 phosphorylation, which also relies on Src activity. A previous study reported that Src indirectly downregulates proteasome activity by activating the p38 MAPK [69]. Our work uncovered that Src directly phosphorylates Rpt2-Y439 and inhibits membrane proteasome activity. This appears to be a biologically relevant arm of saracatinib-elicited cellular responses, as the Rpt2-Y439F mutation in H1975 cells caused partial resistance to saracatinib and markedly different changes at the proteome level (Figs. 5 and 6). More work is needed to verify which of those saracatinib-downregulated proteins in H1975-WT cells are physiological substrates of membrane-anchored proteasomes and responsible for tumor suppression.

In the absence of saracatinib, blocking Y439 phosphorylation did not cause obvious growth defects of the H1975-Y439F cells *in vitro* or *in vivo*. This was likely because the Y→F

substitution could not fully mimic unphopshorylated wild-type Rpt2 but in effect caused a slight decrease of proteasome activity (Fig. 1I, J, Fig. 4F, Supplementary Fig. S1D and Table S6). Missing the OH- group from the strictly conserved Y439 residue, Rpt2-F439 is admittedly not optimal for RP-CP interaction, although there is no better alternative than this mutant for specifically blocking Y439 phosphorylation in cells. Thus, membrane proteasome activity was dampened in both H1975-WT and YF cells but via different mechanisms (Y439 phosphorylation vs. Y439F mutation), which could account for the similar growth rate seen in these cells under basal conditions. However, saracatinib could relieve Src-imposed proteasome inhibition in H1975-WT cells but not in YF cells, hence unmasking the difference between the two. This led to the identification of the 191 proteins differentially regulated by saracatinib between H1975-WT and YF cells (Fig. 5E). Even so, changes of some of these proteins might have resulted indirectly from dysregulation of other proteins in the YF cells, in which not only membrane-associated but almost all proteasomes are affected by the Y→F mutation to some extent (Table S6). Therefore, cautions should be taken when interpreting these data. Nevertheless, the colony formation, tumor xenograft and mass spectrometry assays all support the notion that Rpt2-Y439 phosphorylation is an important determinant of how H1975 cells respond to saracatinib.

In this work, we have confirmed the membrane-associated PTPN2 isoform, TC48, as the first PTP known to bind and regulate the proteasome. We do not exclude the possibility that TC48 and the other PTPN2 isoforms may regulate different pTyr sites of the proteasome, and that there may be other pY439 phosphatase(s) yet to be identified. Multiple PTPs likely act in concert to maintain the low level of proteasome tyrosine phosphorylation in the cell, which may be important for cellular fitness. PTPs have emerged as novel drug targets for treating multiple diseases including diabetes, autoimmune disorders and cancer [25, 26, 70]. Recent studies have demonstrated that deletion of PTPN2 in cancer cells or in T cells greatly boosts immunotherapy by upregulating the JAK/STAT pathway [71–73]. In addition, variants of the *PTPN2* gene that decrease PTPN2 expression were found to be associated with reduced risk of lung cancer [74]. Our data imply that upregulated Rpt2-Y439 phosphorylation following PTPN2 inactivation may exaggerate the impact of activated RTKs/Src on membrane-associated proteasomes and render cancer cells more sensitive to TKIs such as saracatinib. The clinical importance of proteasome tyrosine phosphorylation in cancer treatment warrants further investigation.

Materials and Methods

Immunoblotting, immunoprecipitation and affinity pulldown

Regular immunoblotting, immunoprecipitation and affinity pulldown assays were performed as reported [66]. In assays to examine Y439 phosphorylation by immunoprecipitation of endogenous Rpt2 or Rpt2-IF, cells were lysed without ATP/Mg^{2+} but with 1% SDS and 10 mM activated orthovanadate in addition to other protease/phosphatase inhibitors. Cell lysates were then diluted 10-fold with lysis buffer containing all inhibitors, sonicated and spin-cleared before mixing with anti-Rpt2 or anti-Flag antibodies. All incubation and washing were performed at 4°C.

Animal studies

All animals were purchased from SLAC Laboratory Animal Co., Ltd (Shanghai, China) and studies were conducted in full compliance with policies of the Institutional Animal Care and Use Committee (IACUC) of Zhejiang University. Six-week old female nu/nu mice were housed at the Laboratory Animal Center at Zhejiang University. Four groups of mice (5 per group) were used for tumor xenograft experiments. All mice were of almost identical body weight at the beginning of the experiment and no statistical method was used to predetermine sample size. Each mouse was injected subcutaneously at the flank with 2.0×10^6/100 μl of H1975 cells, which were resuspended in PBS and mixed 1:1 (v/v) with Matrigel (Corning, #354234). Two weeks later, tumor sizes and body weights were similar among all tumor-bearing mice. Mice bearing the same type of H1975 tumor were separated based on their cage number to receive DMSO (odd-numbered cages) or saracatinib (even-numbered cages, 25 mg/kg/d) treatment. Saracatinib was dissolved in DMSO and diluted in PEG300 as recommended by the vendor (Selleckchem), and administered daily by oral gavaging after body weight measurement. Tumor size was measured every other day with a digital caliber, and tumor volume was calculated as V (mm^3) = ½ ($width^2$ x length). At the end of the study, mice were euthanized (none excluded) and tumors were resected out, weighed and immediately frozen in liquid nitrogen then stored at −80°C. Tumor tissues were later Dounce-homogenized in hypotonic lysis buffer (containing protease and phosphatase inhibitors) and sonicated. SDS (0.1% final) was then added to facilitate membrane protein extraction. Tissue lysates were cleared by centrifugation and quantified by BCA protein assay (Thermo Fisher) for western blot analysis.

Pregnant wild-type Sprague Dawley rats were sacrificed and E15.5 embryos were dissected. Forebrain/midbrain tissues were homogenized in TBS buffer supplemented with 1% SDS and protease/phosphatase inhibitors. Tissue homogenates were further diluted and sonicated before anti-Rpt2 immunoprecipitation.

General methods for data analysis

Western blot results were quantified by ImageJ (https://imagej.nih.gov/ij/). Structural models were generated with PyMol and Coot. Sequence alignment was performed by ClustalW. Unless otherwise noted, three independent experiments were used for statistical analyses (by GraphPad Prism), variances were similar between groups and quantitative results are shown as mean ± S.D.

Others

Details of cell culture, plasmids, reagents, microscopy, biochemical assays, proteomic and bioinformatic analyses can be found in the Supplemental Materials. Antibody information is listed in Table S7. Primer/oligonucleotide sequences are shown in Table S8.

Supplementary Material

Refer to Web version on PubMed Central for supplementary material.

Acknowledgements

We thank Drs. Xin-Hua Feng, Hai Song, Bin Zhao (Life Sciences Institute, Zhejiang University, LSI-ZJU), Zhong-Yin Zhang (Purdue University), Shigeo Murata (The University of Tokyo) and Susan Lindquist (Massachusetts Institute of Technology) for crucial constructs, cell lines and reagents. We are grateful for the critical and encouraging comments from Drs. Kun-Liang Guan, Anne-Claude Gingras, Benjamin Neel, Tony Hunter and Tony Tiganis. We appreciate the technical assistance from Xiaorui Jiang, Fei Zhang and the Core Facilities of LSI-ZJU. X.G. was supported by Natural Science Foundation of China (31671391, 31870762), Zhejiang Natural Science Foundation (LR18C050001), Fundamental Research Funds for the Central Universities (2016QN81011), and the startup funding from Zhejiang University. B.Y. was funded by Natural Science Foundation of China (91953103). Z.W. was supported by Natural Science Foundation of China (31671039) and National Key Research and Development Plan of the Ministry of Science and Technology of China (2016YF0501000). L.H. was funded by NIH (R01GM074830).

References

1. Finley D, Prado MA. The Proteasome and Its Network: Engineering for Adaptability. Cold Spring Harbor perspectives in biology 2020; 12: a033985. [PubMed: 30833452]
2. Schmidt M, Finley D. Regulation of proteasome activity in health and disease. Biochimica et biophysica acta 2014; 1843: 13–25. [PubMed: 23994620]
3. Collins GA, Goldberg AL. The Logic of the 26S Proteasome. Cell 2017; 169: 792–806. [PubMed: 28525752]
4. Murata S, Yashiroda H, Tanaka K. Molecular mechanisms of proteasome assembly. Nat Rev Mol Cell Biol 2009; 10: 104–115. [PubMed: 19165213]
5. Budenholzer L, Cheng CL, Li Y, Hochstrasser M. Proteasome Structure and Assembly. Journal of molecular biology 2017; 429: 3500–3524. [PubMed: 28583440]
6. Finley D Recognition and processing of ubiquitin-protein conjugates by the proteasome. Annu Rev Biochem 2009; 78: 477–513. [PubMed: 19489727]
7. Bard JAM, Goodall EA, Greene ER, Jonsson E, Dong KC, Martin A. Structure and Function of the 26S Proteasome. Annu Rev Biochem 2018; 87: 697–724. [PubMed: 29652515]
8. Eisele MR, Reed RG, Rudack T, Schweitzer A, Beck F, Nagy I et al. Expanded Coverage of the 26S Proteasome Conformational Landscape Reveals Mechanisms of Peptidase Gating. Cell Rep 2018; 24: 1301–1315.e1305. [PubMed: 30067984]
9. Smith DM, Chang SC, Park S, Finley D, Cheng Y, Goldberg AL. Docking of the proteasomal ATPases' carboxyl termini in the 20S proteasome's alpha ring opens the gate for substrate entry. Mol Cell 2007; 27: 731–744. [PubMed: 17803938]
10. Park S, Li X, Kim HM, Singh CR, Tian G, Hoyt MA et al. Reconfiguration of the proteasome during chaperone-mediated assembly. Nature 2013; 497: 512–516. [PubMed: 23644457]
11. Park S, Roelofs J, Kim W, Robert J, Schmidt M, Gygi SP et al. Hexameric assembly of the proteasomal ATPases is templated through their C termini. Nature 2009; 459: 866–870. [PubMed: 19412160]
12. Kumar B, Kim YC, DeMartino GN. The C terminus of Rpt3, an ATPase subunit of PA700 (19 S) regulatory complex, is essential for 26 S proteasome assembly but not for activation. J Biol Chem 2010; 285: 39523–39535. [PubMed: 20937828]
13. Guo X, Huang X, Chen MJ. Reversible phosphorylation of the 26S proteasome. Protein & cell 2017; 8: 255–272. [PubMed: 28258412]
14. VerPlank JJS, Goldberg AL. Regulating protein breakdown through proteasome phosphorylation. Biochem J 2017; 474: 3355–3371. [PubMed: 28947610]
15. Li D, Dong Q, Tao Q, Gu J, Cui Y, Jiang X et al. c-Abl regulates proteasome abundance by controlling the ubiquitin-proteasomal degradation of PSMA7 subunit. Cell Rep 2015; 10: 484–496. [PubMed: 25620702]
16. Liu X, Huang W, Li C, Li P, Yuan J, Li X et al. Interaction between c-Abl and Arg tyrosine kinases and proteasome subunit PSMA7 regulates proteasome degradation. Mol Cell 2006; 22: 317–327. [PubMed: 16678104]

17. Hunter T The genesis of tyrosine phosphorylation. Cold Spring Harbor perspectives in biology 2014; 6: a020644. [PubMed: 24789824]
18. Kolch W, Pitt A. Functional proteomics to dissect tyrosine kinase signalling pathways in cancer. Nat Rev Cancer 2010; 10: 618–629. [PubMed: 20720570]
19. Tibes R, Trent J, Kurzrock R. Tyrosine kinase inhibitors and the dawn of molecular cancer therapeutics. Annu Rev Pharmacol Toxicol 2005; 45: 357–384. [PubMed: 15822181]
20. Casaletto JB, McClatchey AI. Spatial regulation of receptor tyrosine kinases in development and cancer. Nat Rev Cancer 2012; 12: 387–400. [PubMed: 22622641]
21. Sharma K, D'Souza RC, Tyanova S, Schaab C, Wisniewski JR, Cox J et al. Ultradeep human phosphoproteome reveals a distinct regulatory nature of Tyr and Ser/Thr-based signaling. Cell Rep 2014; 8: 1583–1594. [PubMed: 25159151]
22. Alonso A, Sasin J, Bottini N, Friedberg I, Friedberg I, Osterman A et al. Protein tyrosine phosphatases in the human genome. Cell 2004; 117: 699–711. [PubMed: 15186772]
23. Sun H, Tonks NK. The coordinated action of protein tyrosine phosphatases and kinases in cell signaling. Trends Biochem Sci 1994; 19: 480–485. [PubMed: 7855891]
24. Julien SG, Dubé N, Hardy S, Tremblay ML. Inside the human cancer tyrosine phosphatome. Nat Rev Cancer 2011; 11: 35–49. [PubMed: 21179176]
25. Frankson R, Yu ZH, Bai Y, Li Q, Zhang RY, Zhang ZY. Therapeutic Targeting of Oncogenic Tyrosine Phosphatases. Cancer Res 2017; 77: 5701–5705. [PubMed: 28855209]
26. Zhang ZY. Drugging the Undruggable: Therapeutic Potential of Targeting Protein Tyrosine Phosphatases. Accounts of chemical research 2017; 50: 122–129. [PubMed: 27977138]
27. Thinon E, Serwa RA, Broncel M, Brannigan JA, Brassat U, Wright MH et al. Global profiling of co- and post-translationally N-myristoylated proteomes in human cells. Nature communications 2014; 5: 4919.
28. Muppirala M, Gupta V, Swarup G. Emerging role of tyrosine phosphatase, TCPTP, in the organelles of the early secretory pathway. Biochimica et biophysica acta 2013; 1833: 1125–1132. [PubMed: 23328081]
29. Guerrero C, Milenkovic T, Przulj N, Kaiser P, Huang L. Characterization of the proteasome interaction network using a QTAX-based tag-team strategy and protein interaction network analysis. Proc Natl Acad Sci U S A 2008; 105: 13333–13338. [PubMed: 18757749]
30. Guo X, Wang X, Wang Z, Banerjee S, Yang J, Huang L et al. Site-specific proteasome phosphorylation controls cell proliferation and tumorigenesis. Nat Cell Biol 2016; 18: 202–212. [PubMed: 26655835]
31. Huang X, Luan B, Wu J, Shi Y. An atomic structure of the human 26S proteasome. Nature structural & molecular biology 2016; 23: 778–785.
32. Shibahara T, Kawasaki H, Hirano H. Identification of the 19S regulatory particle subunits from the rice 26S proteasome. Eur J Biochem 2002; 269: 1474–1483. [PubMed: 11874462]
33. Kimura Y, Saeki Y, Yokosawa H, Polevoda B, Sherman F, Hirano H. N-Terminal modifications of the 19S regulatory particle subunits of the yeast proteasome. Arch Biochem Biophys 2003; 409: 341–348. [PubMed: 12504901]
34. Kimura A, Kato Y, Hirano H. N-myristoylation of the Rpt2 subunit regulates intracellular localization of the yeast 26S proteasome. Biochemistry 2012; 51: 8856–8866. [PubMed: 23102099]
35. Kimura A, Kurata Y, Nakabayashi J, Kagawa H, Hirano H. N-Myristoylation of the Rpt2 subunit of the yeast 26S proteasome is implicated in the subcellular compartment-specific protein quality control system. J Proteomics 2016; 130: 33–41. [PubMed: 26344132]
36. Zong C, Gomes AV, Drews O, Li X, Young GW, Berhane B et al. Regulation of murine cardiac 20S proteasomes: role of associating partners. Circ Res 2006; 99: 372–380. [PubMed: 16857963]
37. Wang X, Chen CF, Baker PR, Chen PL, Kaiser P, Huang L. Mass spectrometric characterization of the affinity-purified human 26S proteasome complex. Biochemistry 2007; 46: 3553–3565. [PubMed: 17323924]
38. Kikuchi J, Iwafune Y, Akiyama T, Okayama A, Nakamura H, Arakawa N et al. Co- and post-translational modifications of the 26S proteasome in yeast. Proteomics 2010; 10: 2769–2779. [PubMed: 20486117]

39. Albert S, Schaffer M, Beck F, Mosalaganti S, Asano S, Thomas HF et al. Proteasomes tether to two distinct sites at the nuclear pore complex. Proc Natl Acad Sci U S A 2017; 114: 13726–13731. [PubMed: 29229809]
40. Ramachandran KV, Margolis SS. A mammalian nervous-system-specific plasma membrane proteasome complex that modulates neuronal function. Nature structural & molecular biology 2017; 24: 419–430.
41. Rivett AJ, Palmer A, Knecht E. Electron microscopic localization of the multicatalytic proteinase complex in rat liver and in cultured cells. The journal of histochemistry and cytochemistry : official journal of the Histochemistry Society 1992; 40: 1165–1172. [PubMed: 1619280]
42. Kohn AD, Summers SA, Birnbaum MJ, Roth RA. Expression of a constitutively active Akt Ser/Thr kinase in 3T3-L1 adipocytes stimulates glucose uptake and glucose transporter 4 translocation. J Biol Chem 1996; 271: 31372–31378. [PubMed: 8940145]
43. Moritz A, Li Y, Guo A, Villen J, Wang Y, MacNeill J et al. Akt-RSK-S6 kinase signaling networks activated by oncogenic receptor tyrosine kinases. Science signaling 2010; 3: ra64. [PubMed: 20736484]
44. Cross DA, Ashton SE, Ghiorghiu S, Eberlein C, Nebhan CA, Spitzler PJ et al. AZD9291, an irreversible EGFR TKI, overcomes T790M-mediated resistance to EGFR inhibitors in lung cancer. Cancer discovery 2014; 4: 1046–1061. [PubMed: 24893891]
45. Wang J, Gray NS. SnapShot: Kinase Inhibitors II. Mol Cell 2015; 58: 710.e711.
46. Kamps MP, Buss JE, Sefton BM. Mutation of NH2-terminal glycine of p60src prevents both myristoylation and morphological transformation. Proc Natl Acad Sci U S A 1985; 82: 4625–4628. [PubMed: 2991884]
47. Li X, Zhao X, Fang Y, Jiang X, Duong T, Fan C et al. Generation of destabilized green fluorescent protein as a transcription reporter. J Biol Chem 1998; 273: 34970–34975. [PubMed: 9857028]
48. Hein MY, Hubner NC, Poser I, Cox J, Nagaraj N, Toyoda Y et al. A human interactome in three quantitative dimensions organized by stoichiometries and abundances. Cell 2015; 163: 712–723. [PubMed: 26496610]
49. St-Denis N, Gupta GD, Lin ZY, Gonzalez-Badillo B, Veri AO, Knight JDR et al. Phenotypic and Interaction Profiling of the Human Phosphatases Identifies Diverse Mitotic Regulators. Cell Rep 2016; 17: 2488–2501. [PubMed: 27880917]
50. Kumar P, Munnangi P, Chowdary KR, Shah VJ, Shinde SR, Kolli NR et al. A Human Tyrosine Phosphatase Interactome Mapped by Proteomic Profiling. J Proteome Res 2017; 16: 2789–2801. [PubMed: 28675297]
51. van Vliet C, Bukczynska PE, Puryer MA, Sadek CM, Shields BJ, Tremblay ML et al. Selective regulation of tumor necrosis factor-induced Erk signaling by Src family kinases and the T cell protein tyrosine phosphatase. Nature immunology 2005; 6: 253–260. [PubMed: 15696169]
52. Zhang S, Chen L, Luo Y, Gunawan A, Lawrence DS, Zhang ZY. Acquisition of a potent and selective TC-PTP inhibitor via a stepwise fluorophore-tagged combinatorial synthesis and screening strategy. Journal of the American Chemical Society 2009; 131: 13072–13079. [PubMed: 19737019]
53. Ye DZ, Field J. PAK signaling in cancer. Cellular logistics 2012; 2: 105–116. [PubMed: 23162742]
54. Zhen Y, Chunlei G, Wenzhi S, Shuangtao Z, Na L, Rongrong W et al. Clinicopathologic significance of legumain overexpression in cancer: a systematic review and meta-analysis. Scientific reports 2015; 5: 16599. [PubMed: 26607955]
55. Simanshu DK, Nissley DV, McCormick F. RAS Proteins and Their Regulators in Human Disease. Cell 2017; 170: 17–33. [PubMed: 28666118]
56. Alevizopoulos K, Calogeropoulou T, Lang F, Stournaras C. Na+/K+ ATPase inhibitors in cancer. Current drug targets 2014; 15: 988–1000. [PubMed: 25198786]
57. Formisano L, D'Amato V, Servetto A, Brillante S, Raimondo L, Di Mauro C et al. Src inhibitors act through different mechanisms in Non-Small Cell Lung Cancer models depending on EGFR and RAS mutational status. Oncotarget 2015; 6: 26090–26103. [PubMed: 26325669]
58. Tanaka K, Fujiwara T, Kumatori A, Shin S, Yoshimura T, Ichihara A et al. Molecular cloning of cDNA for proteasomes from rat liver: primary structure of component C3 with a possible tyrosine phosphorylation site. Biochemistry 1990; 29: 3777–3785. [PubMed: 2340272]

59. Hemmis CW, Heard SC, Hill CP. Phosphorylation of Tyr-950 in the proteasome scaffolding protein RPN2 modulates its interaction with the ubiquitin receptor RPN13. J Biol Chem 2019; 294: 9659–9665. [PubMed: 31064842]
60. Tang M, Lu X, Zhang C, Du C, Cao L, Hou T et al. Downregulation of SIRT7 by 5-fluorouracil induces radiosensitivity in human colorectal cancer. Theranostics 2017; 7: 1346–1359. [PubMed: 28435470]
61. Scott JD, Pawson T. Cell signaling in space and time: where proteins come together and when they're apart. Science 2009; 326: 1220–1224. [PubMed: 19965465]
62. Manning G, Whyte DB, Martinez R, Hunter T, Sudarsanam S. The protein kinase complement of the human genome. Science 2002; 298: 1912–1934. [PubMed: 12471243]
63. Kim YC, DeMartino GN. C termini of proteasomal ATPases play nonequivalent roles in cellular assembly of mammalian 26 S proteasome. J Biol Chem 2011; 286: 26652–26666. [PubMed: 21628461]
64. Murata S, Takahama Y, Kasahara M, Tanaka K. The immunoproteasome and thymoproteasome: functions, evolution and human disease. Nature immunology 2018; 19: 923–931. [PubMed: 30104634]
65. Bose S, Brooks P, Mason GG, Rivett AJ. gamma-Interferon decreases the level of 26 S proteasomes and changes the pattern of phosphorylation. Biochem J 2001; 353: 291–297. [PubMed: 11139393]
66. Liu X, Xiao W, Zhang Y, Wiley SE, Zuo T, Zheng Y et al. Reversible phosphorylation of Rpn1 regulates 26S proteasome assembly and function. Proc Natl Acad Sci U S A 2020; 117: 328–336. [PubMed: 31843888]
67. Lokireddy S, Kukushkin NV, Goldberg AL. cAMP-induced phosphorylation of 26S proteasomes on Rpn6/PSMD11 enhances their activity and the degradation of misfolded proteins. Proc Natl Acad Sci U S A 2015; 112: E7176–7185. [PubMed: 26669444]
68. Satoh K, Sasajima H, Nyoumura K-i, Yokosawa H, Sawada H. Assembly of the 26S Proteasome Is Regulated by Phosphorylation of the p45/Rpt6 ATPase Subunit. Biochemistry 2000; 40: 314–319.
69. Heun Y, Grundler Groterhorst K, Pogoda K, Kraemer BF, Pfeifer A, Pohl U et al. The Phosphatase SHP-2 Activates HIF-1α in Wounds In Vivo by Inhibition of 26S Proteasome Activity. International journal of molecular sciences 2019; 20: 4404–4416.
70. Barr AJ. Protein tyrosine phosphatases as drug targets: strategies and challenges of inhibitor development. Future medicinal chemistry 2010; 2: 1563–1576. [PubMed: 21426149]
71. Wei J, Long L, Zheng W, Dhungana Y, Lim SA, Guy C et al. Targeting REGNASE-1 programs long-lived effector T cells for cancer therapy. Nature 2019; 576: 471–476. [PubMed: 31827283]
72. Manguso RT, Pope HW, Zimmer MD, Brown FD, Yates KB, Miller BC et al. In vivo CRISPR screening identifies Ptpn2 as a cancer immunotherapy target. Nature 2017; 547: 413–418. [PubMed: 28723893]
73. Wiede F, Lu KH, Du X, Liang S, Hochheiser K, Dodd GT et al. PTPN2 phosphatase deletion in T cells promotes anti-tumour immunity and CAR T-cell efficacy in solid tumours. Embo j 2020; 39: e103637. [PubMed: 31803974]
74. Feng Y, Wang Y, Liu H, Liu Z, Mills C, Han Y et al. Genetic variants of PTPN2 are associated with lung cancer risk: a re-analysis of eight GWASs in the TRICL-ILCCO consortium. Scientific reports 2017; 7: 825. [PubMed: 28400551]

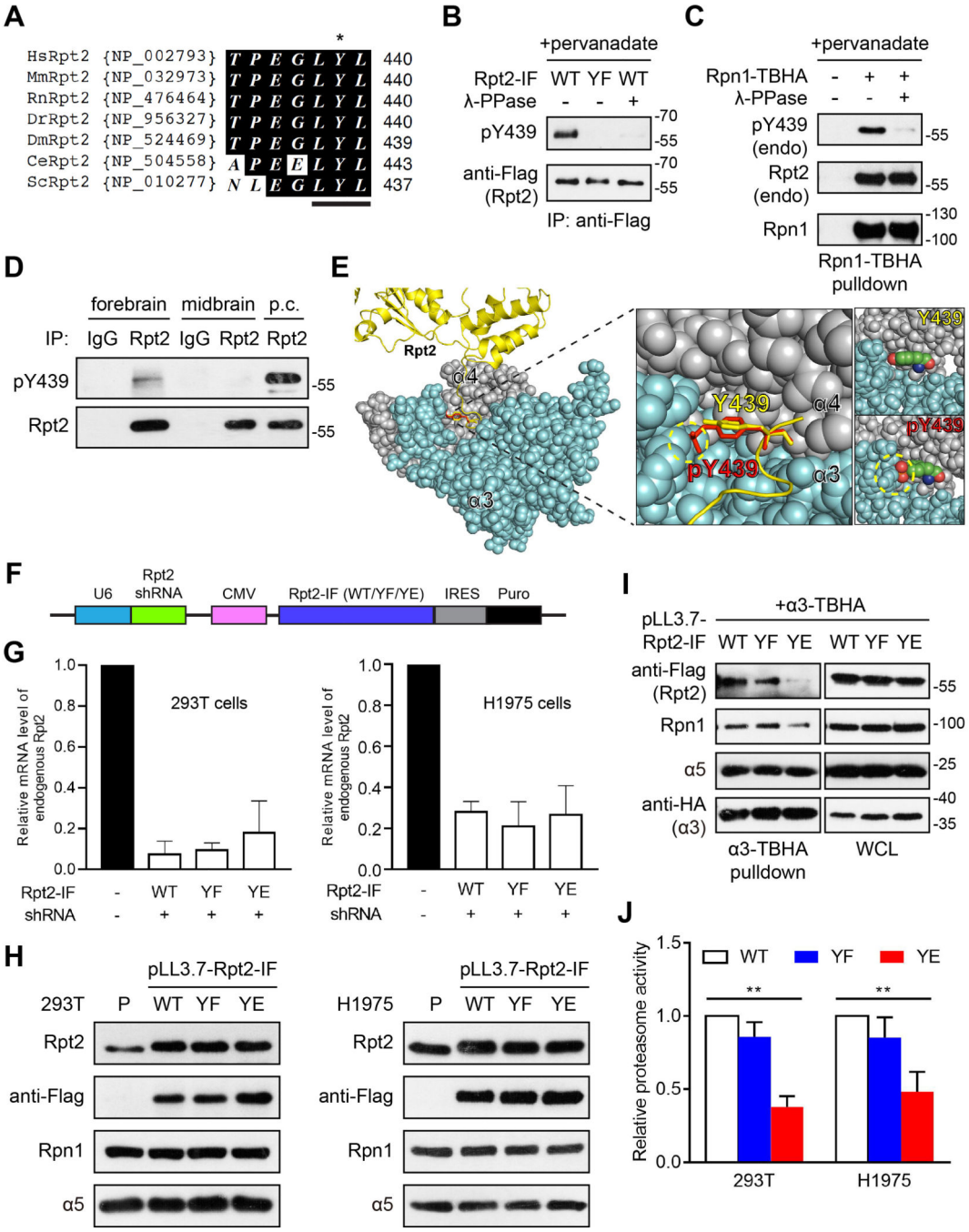

Fig. 1. Rpt2-Y439 phosphorylation perturbs 26S proteasome function.

A. Sequence alignment of the C-termini of Rpt2 from different species. The HbYX motif (LYL, underlined) including Y439 (*) is strictly conserved through evolution.

B. 293T cells were transfected with the indicated variants of Rpt2-IF (internal Flag) and treated with pervanadate (0.1 mM, 15 min) before lysis. After anti-Flag immunoprecipitation, samples were treated with or without λ-phosphatase and probed with the indicated antibodies. YF, Y439F.

C. 293T cells were transfected with Rpn1-TBHA, treated with pervanadate as in (B) and lysed for streptavidin pulldown. Samples were treated with or without λ-phosphatase and endogenous Rpt2 was probed with the indicated antibodies.

D. The indicated brain regions were dissected from E15.5 rat embryos. Tissue samples were lysed under denaturing conditions (1% SDS). Diluted homogenates were incubated with a control rabbit IgG or anti-Rpt2 antibody for immunoprecipitation followed by western blot. p.c., positive control (endogenous Rpt2 immunoprecipitated from pervanadate-treated H1975 cells).

E. Structural modeling of Rpt2-Y439 phosphorylation. (Left and middle) Rpt2 is shown as yellow ribbons. Y439 and pY439 are modeled as yellow and red sticks, respectively. The dotted yellow circle indicates the steric clash between the phosphate group of pY439 and α3 (cyan spheres). (Right) Sphere presentation of Y439 and pY439 atoms, with O, C and N shown as red, green and blue, respectively. The model was built on the 26S proteasome structure 6MSJ (PDB ID) and further adjusted in Coot.

F. Schematic of the pLL3.7-Rpt2 construct for simultaneously knocking down endogenous Rpt2 and re-expressing Rpt2-IF variants.

G. qPCR measurement of endogenous Rpt2 mRNA in 293T and H1975 cells stably transduced with pLL3.7-Rpt2 shown in (F), n = 3 for each cell type.

H. Western blot verification of exogenous Rpt2-IF expression in the above 293T and H1975 cells.

I. α3-TBHA was transiently expressed in 293T cells as in (G) and (H) for streptavidin pulldown and western blot analysis. WCL, whole cell lysate.

J. 293T and H1975 cells as in (G) and (H) were lysed for proteasome activity measurement using Suc-LLVY-AMC as substrate. **, $P < 0.01$ (One-way ANOVA, n = 3). Paired comparisons: 293T WT vs. YF, $P = 0.2012$; 293T WT vs. YE, $P = 0.0070$. H1975 WT vs. YF, $P = 0.3045$; H1975 WT vs. YE, $P = 0.0341$.

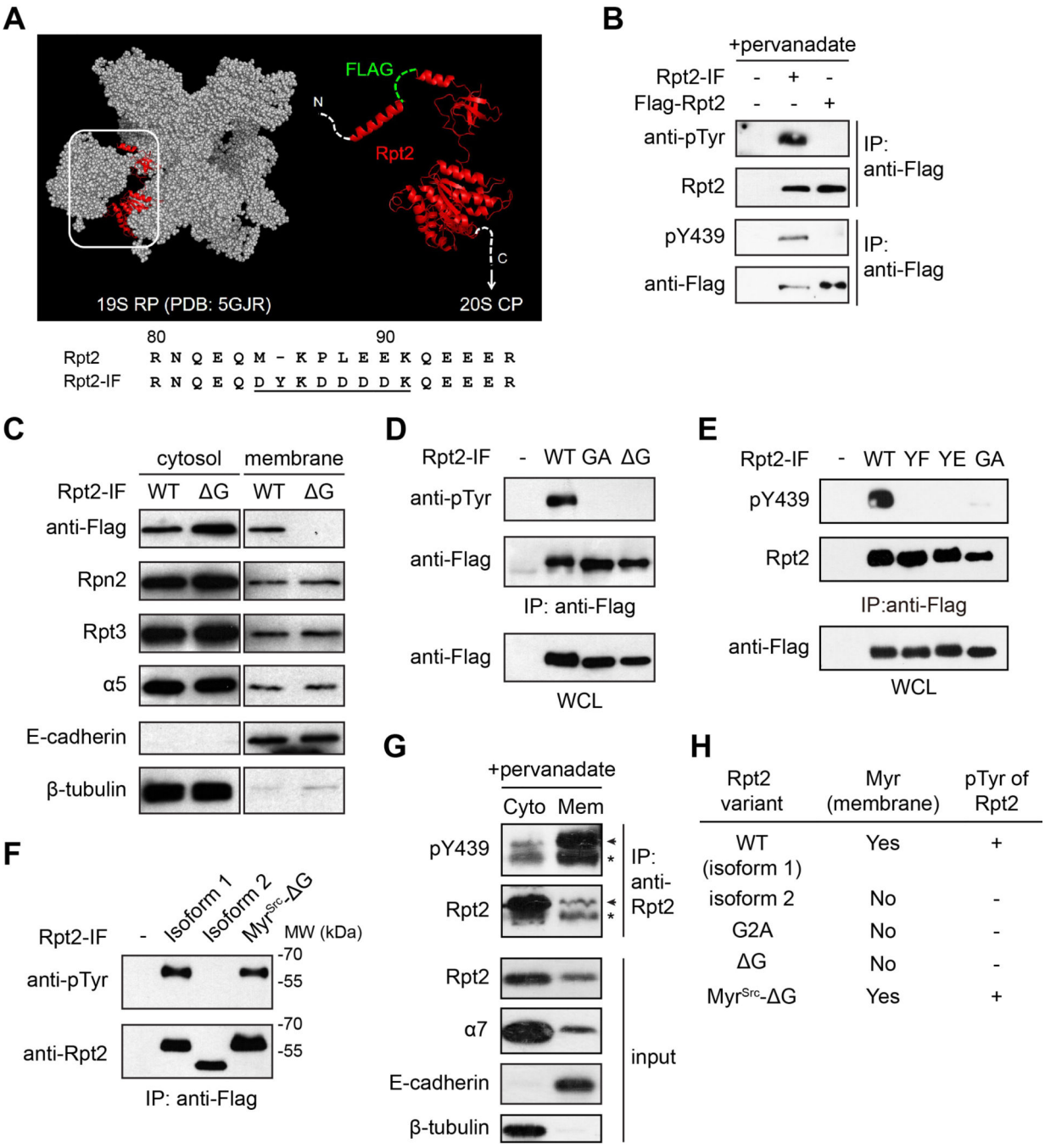

Fig. 2. Rpt2 membrane localization is required for its tyrosine phosphorylation.

A. In the cyro-EM structure of the 19S RP (grey spheres, top), Rpt2 (red ribbons) contains a flexible region (aa. 85–91, green dotted line), which was replaced with DYKDDDDK (Flag tag) to generate Rpt2-IF (bottom).

B. Rpt2-IF and N-terminally tagged Flag-Rpt2 were transiently expressed in 293T cells. After pervanadate treatment, exogenous Rpt2 was immunoprecipitated and examined for total tyrosine phosphorylation or pY439 using the indicated antibodies.

C. Rpt2-IF-WT and the myristoylation-deficient mutant Rpt2-IF-ΔG were ectopically expressed in 293T cells. Cytosolic and membrane fractions were separated and probed with the indicated antibodies. E-cadherin and β-tubulin served as membrane and cytosolic markers, respectively.

D. The indicated Rpt2-IF constructs were transiently expressed in 293T cells. After pervanadate treatment, cells were lysed under denaturing conditions. After dilution, Rpt2 variants were enriched by anti-Flag immunoprecipitation and probed for pTyr. GA, G2A.

E. The indicated Rpt2-IF variants were expressed, immunoprecipitated as in (D) and blotted with anti-pY439 antibody.

F. The indicated Rpt2-IF variants were expressed, immunoprecipitated and blotted as in (D). Isoform 1 is the same full-length Rpt2-IF-WT used elsewhere. Isoform 2 lacks aa. 1–73 of isoform 1.

G. H1975 cells were treated with pervanadate and fractionated. Membrane proteins were extracted with TBS buffer plus 1% SDS then diluted. Equal amounts of cytosolic and membrane fractions were used for immunoprecipitation of endogenous Rpt2. pY439 and Rpt2 were probed (arrowheads). *, non-specific band.

H. Summary of results from (D) to (F), highlighting the dependence of Rpt2 tyrosine phosphorylation on its membrane localization.

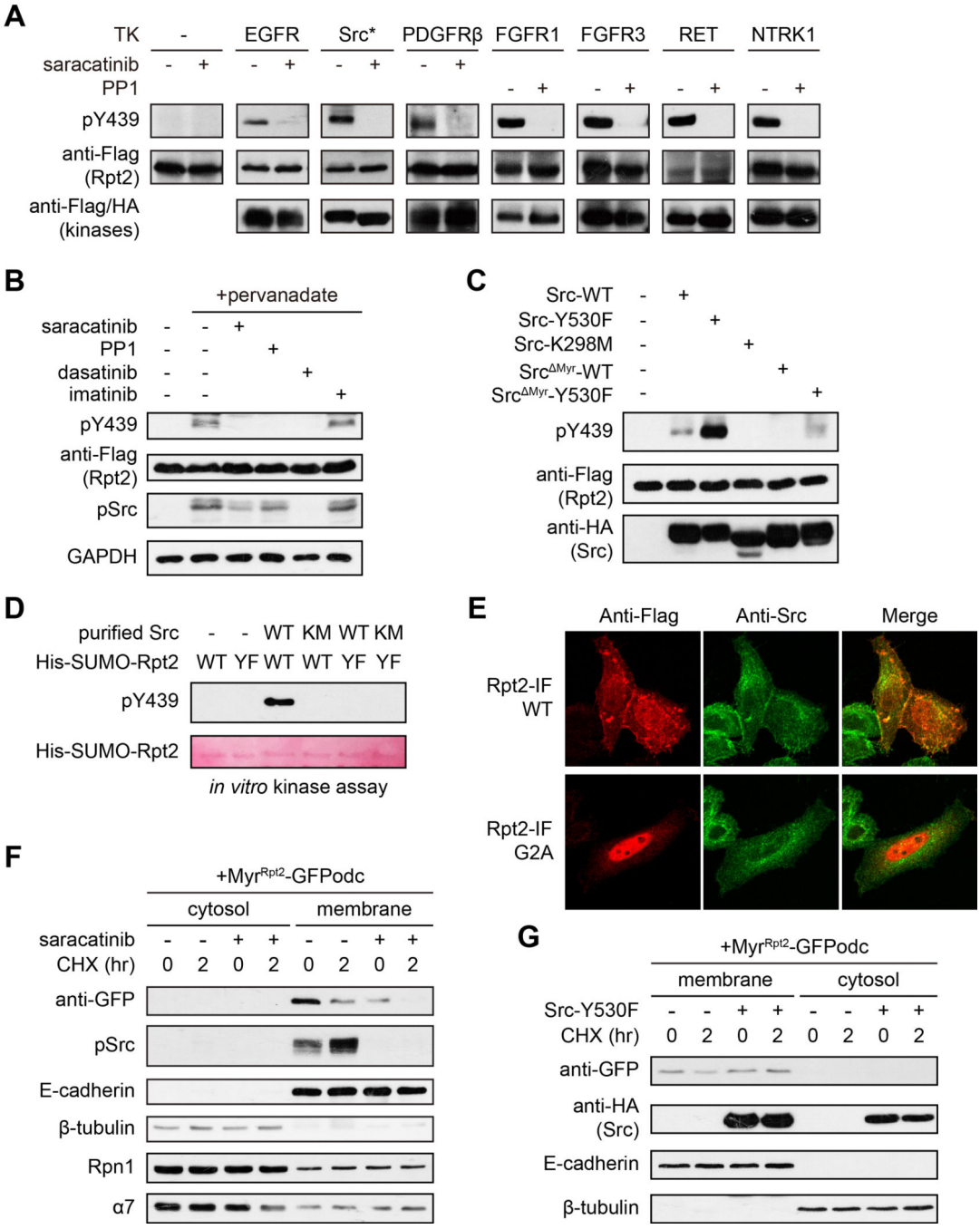

Fig. 3. Src phosphorylates Rpt2-Y439.

A. 293T pLL3.7-Rpt2-IF-WT cells transfected with vector control or the indicated tyrosine kinases (TKs) were treated with DMSO (−) or the indicated Src inhibitors (5 μM, 1 h) before harvest. Whole cell lysates were immediately denatured and probed with the antibodies shown. Src*, Src-Y530F-TBHA. All other TKs contain a C-terminal 3xFlag-V5 tag.

B. 293T pLL3.7-Rpt2-IF-WT cells were treated with DMSO (−) or different inhibitors (5 μM, 1 h). Pervanadate was added at 15 min before harvest. Whole cell lysates were immediately denatured and probed with the indicated antibodies. pSrc, Src-pY419.

C. 293T pLL3.7-Rpt2-IF-WT cells were transfected with vector control or variants of Src-TBHA. Whole cell lysates were immediately denatured and probed with the indicated antibodies.

D. Purified Src (WT or K298M) was incubated with recombinant His-SUMO-Rpt2 protein (WT or Y439F) for an *in vitro* kinase assay. Y439 phosphorylation was examined by western blot, and equal loading of His-SUMO-Rpt2 was shown by Ponceau S staining of the membrane.

E. HeLa cells were transfected with Rpt2-IF (WT or G2A), stained with anti-Flag and anti-Src (endogenous) antibodies and imaged with a con-focal fluorescence microscope. Image size: X = Y = 500 pixels, 68.75 μm.

F. A single clone of 293T cells stably expressing mCherry-IRES-Myr^{Rpt2}-GFPodc were treated with DMSO or saracatinib (5 μM, 4 h). Before harvest, cells were treated with cycloheximide (CHX, 50 μg/ml) for the indicated time. After cell fractionation, the indicated proteins were examined by western blot. Quantification of additional repeats is shown in Supplementary Fig. S3H. The mRNA leve of the reporter gene was not affected by saracatinib (fold-change = 1.02 ± 0.08, $p = 0.69$, n = 3).

G. The same reporter cell line was transfected with vector or Src-Y530F-TBHA. CHX was added and cells were processed as in (F). Quantification of additional repeats is shown in Supplementary Fig. S3H.

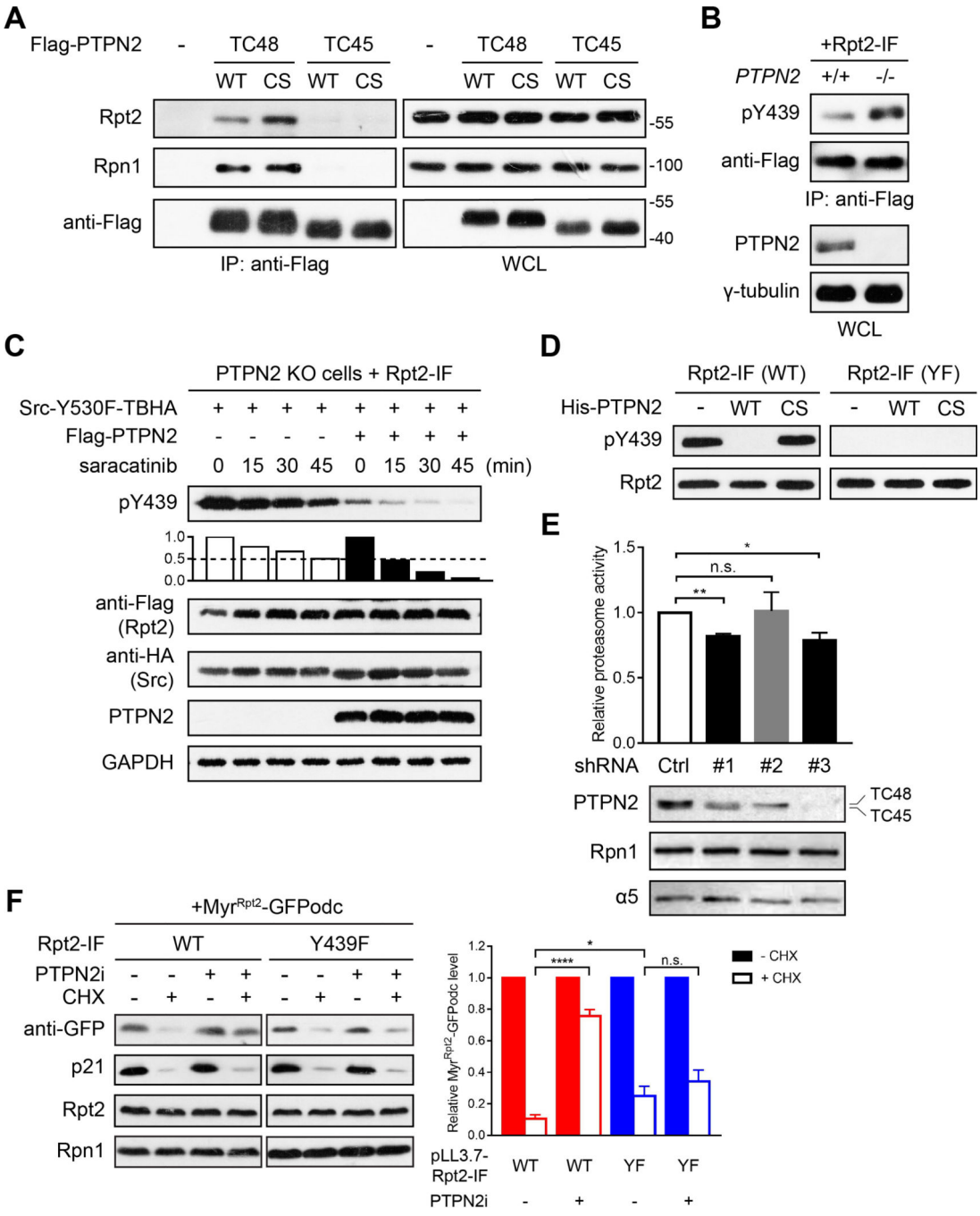

Fig. 4. Rpt2-pY439 is dephosphorylated by PTPN2.

A. Flag-PTPN2 isoforms were expressed in 293T cells. Co-immunoprecipitation of PTPN2 and endogenous proteasome subunits was determined by western blot. CS, C216S.

B. Rpt2-IF was expressed in parental (+/+) or PTPN2-null (−/−) HeLa cells. After anti-Flag immunoprecipitation, pY439 was probed.

C. PTPN2-null 293T cells were co-transfected with Rpt2-IF and activated Src plus vector control or Flag-PTPN2 (TC48). Saracatinib (100 nM) was added at the indicated time points before cell lysis. Whole cell lysates were probed with the indicated antibodies, and

normalized levels of pY439 in each group (against time "0") are shown. Open bars, vector control. Filled bars, TC48-transfected cells.

D. Rpt2-IF-WT/Y439F was immunoprecipitated from pervanadate-treated 293T cells and incubated with bacterially purified His-PTPN2-WT/C216S in an *in vitro* phosphatase assay. Samples were blotted with the indicated antibodies.

E. 293T cells were transfected with a scrambled control shRNA or three independent shRNAs targeting PTPN2. shRNA #1 specifically targets the 3'-UTR of TC48, #2 specifically targets the 3'-UTR of TC45, and #3 targets the coding sequence shared by the two isoforms. Whole cell lysates were used for proteasome activity measurement using Suc-LLVY-AMC as substrate. Knockdown efficiency was verified by the anti-PTPN2 blot. Rpn1 and α5 served as loading control. **, $P < 0.01$; *, $P < 0.05$; n.s., not significant (Student's *t* test vs. control, n = 3).

F. The same Myr^{Rpt2}-GFPodc reporter line as in Fig. 3 was stably transduced with pLL3.7-Rpt2-IF-WT or Y439F. Cells were pretreated with PTPN2 inhibitor (Compound 8, 50 nM) or vehicle (ethanol) for 1 h before CHX treatment (3 h). Whole cell lysates were probed with the indicated antibodies. Representative blots are shown on the left, and normalized Myr^{Rpt2}-GFPodc levels from three independent experiments are shown on the right (filled bars, no CHX; open bars, with CHX). ****, $P < 0.0001$; *, $P < 0.05$; n.s., not significant (Student's *t* test). Note that degradation of a non-membrane substrate of the proteasome, $p21^{Cip1}$, was unaltered by the same treatment.

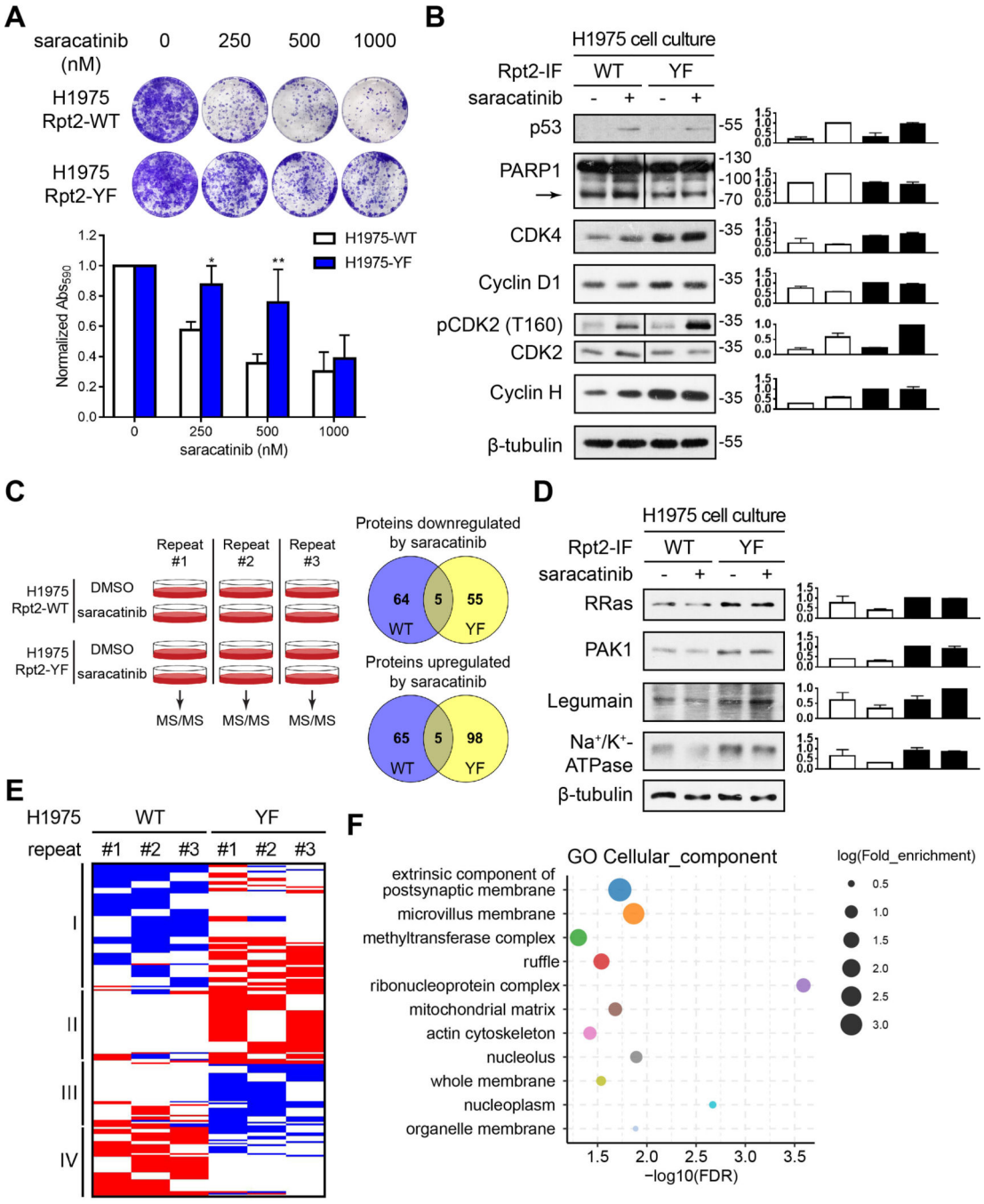

Fig. 5. Altered responses to saracatinib in Rpt2-Y439F cells.

A. Colony formation assays of H1975 cells transduced with pLL3.7-Rpt2-IF-WT or Y439F. Crystal violet-stained cells were photographed (top) and quantified (bottom). *, $P < 0.05$; **, $P < 0.01$ (unpaired two-tailed Student's *t*-test, WT vs. YF, n = 3).

B. H1975-WT/YF cells were treated with DMSO or saracatinib (250 nM) for 24 h. The indicated endogenous proteins were probed from whole cell extracts. Representative blots are shown on the left. Arrow, cleaved PARP1. Results from 3 independent blots of each protein were quantified and shown on the right.

C. Left: The experimental setup for proteomic studies of H1975-WT/YF cells treated with DMSO or saracatinib (250 nM, 24 h). Right: Venn diagrams showing proteins that were downregulated (top) and upregulated (bottom) from each cell line in at least 2 of the 3 biological repeats.

D. Western blot analysis of representative membrane-associated proteins differentially affected by saracatinib in H1975-WT and YF cells. Results from 3 independent blots of each protein were quantified and shown on the right.

E. Heat map visualization of the 191 proteins that responded differently to saracatinib in H1975-WT and YF cells as revealed by mass spectrometry. Each protein in each repeat is represented by a horizontal line. Blue, downregulated by saracatinib (D = −1); red, upregulated by saracatinib (D = 1); white, unchanged by saracatinib (D = 0).

F. Gene Ontology (GO) term analysis showing cellular components enriched among the 191 differentially regulated proteins. Only first-level terms in each hierarchy (indicated by a different color) with FDR < 0.05 are shown.

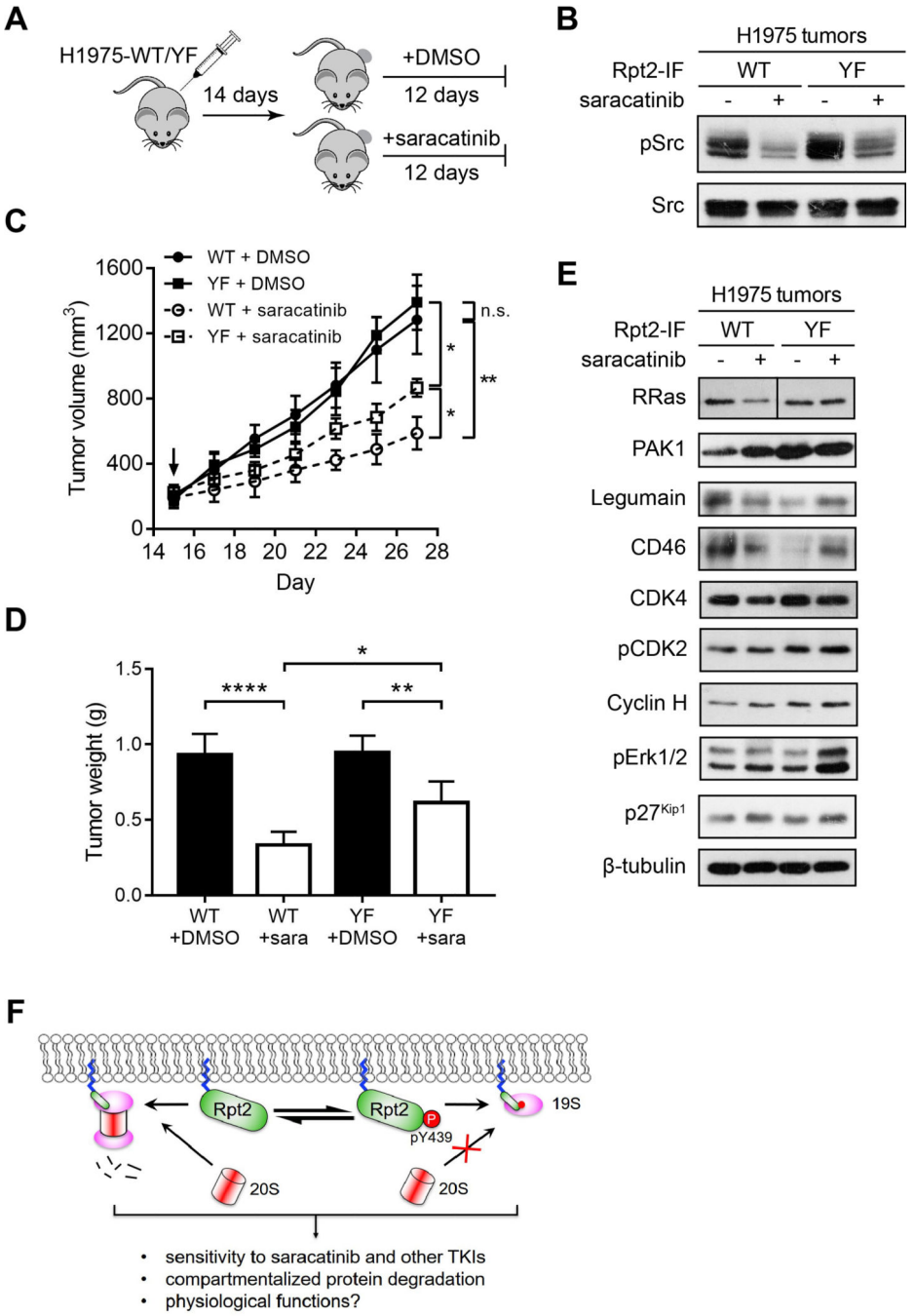

Fig. 6. H1975-Y439F tumors were less inhibited by saracatinib.

A. Schematic of mouse xenograft study with H1975-WT/YF cells.

B. Tumors were dissected at the end of the study, homogenized and probed with the indicated antibodies to demonstrate effective Src inhibition by saracatinib treatment.

C. Growth curves of tumors from the start of DMSO/saracatinib treatment (downward arrow). *, $P < 0.05$; **, $P < 0.01$ (unpaired two-tailed Student's *t*-test between the indicated groups, n = 5). n.s., not significant.

D. Tumor weight measurement. *, $P < 0.05$; **, $P < 0.01$; ****, $P < 0.0001$ (unpaired two-tailed Student's *t*-test between the indicated groups, n = 5).

E. Tumors were processed as in (B) and extracts were blotted with the indicated antibodies.

F. Y439 phosphorylation of membrane-tethered Rpt2 affects 26S proteasome activity at the membrane and cellular responses to Src inhibition by saracatinib.